Defect and Diffusion Forum Vol. 333 (2013) pp 175-192
Online available since 2013/Jan/25 at www.scientific.net

doi:10.4028/www.scientific.net/DDF.333.175

Pseudopartial Grain Boundary Wetting: Key to the Thin Intergranular Layers

B.B. Straumal[1-3,a], A.O. Rodin[2,b], A.E. Shotanov[1,c], A.B. Straumal[2,4,d], O.A. Kogtenkova[1,e], B. Baretzky[3,d]

[1]Institute of Solid State Physics, Russian Academy of Sciences, Ac. Ossipyan str. 2, 142432 Chernogolovka, Russia

[2]National Research Technological University "MISiS", Leninsky prosp. 4, 119991 Moscow, Russia

[3]Karlsruhe Institute for Technology (KIT), Institute for Nanotechnology, Hermann-von-Helmholtz-Platz 1, 76344 Eggenstein-Leopoldshafen, Germany

[4] Lehrstuhl Werkstoffwissenschaft, Institut für Werkstoffe, Fakultät für Maschinenbau, Ruhr-Universität Bochum, Universitätsstr. 150, Geb. IA 1/28, 44801 Bochum, Germany

[a]straumal@issp.ac.ru, [b]rodin@misis.ru, [c]azamatESh@yandex.ru, [d]Alexander.Straumal@rub.de, [e]koololga@issp.ac.ru, [d]brigitte.baretzky@kit.edu

Keywords: Grain boundary wetting, intergranular layers

Abstract. The thin layers of a second phase (also called complexions) in grain boundaries (GB) and triple junctions (TJs) are more and more frequently observed in polycrystals. The prewetting (or premelting) phase transitions were the first phenomena proposed to explain their existence. The deficit of the wetting phase in case of complete wetting can also lead to the formation of thin GB and TJ phases. However, only the phenomenon of pseudopartial (or pseudoincomplete, or constrained complete) wetting permitted to explain, how the thin GB film can exist in the equilibrium with GB lenses of a second phase with non-zero contact angle.

Introduction

The unique properties of the nanostructured materials are of great importance for various advanced applications. The developments of last decade show that these properties are critically controlled by the behavior of grain boundaries (GBs) and triple junctions (TJs) [1, 2]. Moreover, the most advanced experimental methods like high-resolution electron microscopy (HREM) and atom probe microscopy allowed observing that GBs and TJs are frequently not atomically thin and smooth but contain the few nm thick layers or so-called complexions [3–15]. These layers can appear in equilibrium, non-equilibrium (transient) or steady-state structures [4–22]. The goal of this paper is to review the main classes of these GB and TJ phenomena.

Thermodynamic reasons for the existence of GB and TJ thin layers

Let us consider a partially melted two- or multicomponent polycrystal. In this case its temperature is between the solidus temperature T_S and the liquidus temperature T_L, in the equilibrium phase diagram. Consider the droplet of a liquid phase on the surface of a solid phase or between two solid grains. Usually one distinguishes partial and complete wetting of surfaces or interfaces. If a liquid droplet partially wets a solid surface (Fig. 1a) then $\sigma_{sg} - \sigma_{sl} = \sigma_{lg} \cos\theta$, where σ_{sg} is the free energy of solid/gas interface, σ_{sl} is the free energy of solid/liquid interface, σ_{lg} is that of liquid/gas interface and θ is the contact angle. If a liquid droplet partially wets the boundary between two solid grains (Fig. 1b), then $\sigma_{gb} = 2\,\sigma_{sl} \cos\theta$, where σ_{gb} is the free energy of a grain boundary (GB). The free surface or GB which is not covered by the liquid droplets remains dry and contains only the adsorbed atoms with coverage below one monolayer. In this case the GB can exist in the equilibrium contact with the liquid phase (GBs marked with a letter A in Fig. 2b). In the case of

complete wetting (Figs. 1c,d) $\sigma_{sg} > \sigma_{lg} + \sigma_{sl}$ or $\sigma_{gb} > 2\,\sigma_{sl}$, the contact angle is zero, and liquid spreads over the free surface or between grains. In this case the GB separating the grains is completely substituted by the liquid phase (GBs marked with a letter B in Fig. 2b). The GB wetting phenomena are particularly important for the liquid phase sintering or the description of melt infiltration into rocks [23–25].

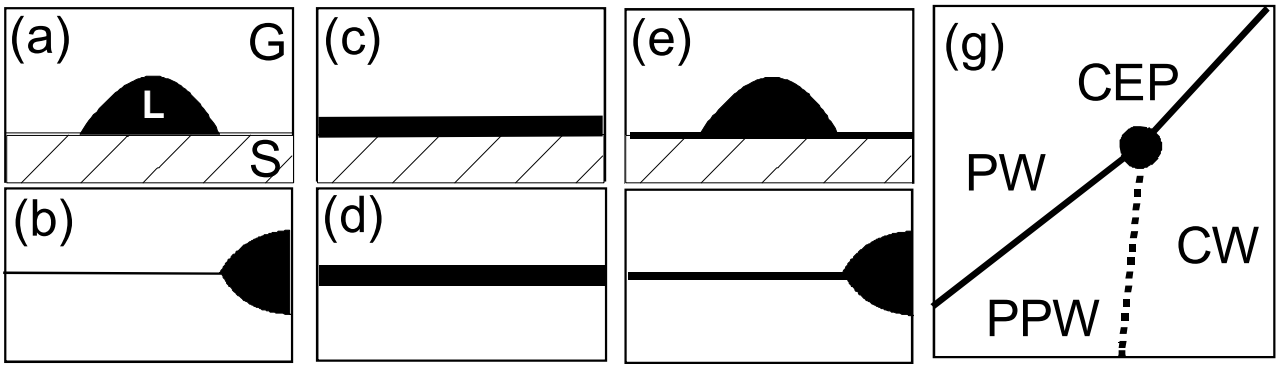

Fig. 1. The schemes for the wetting of free surfaces and GBs. (a) partial surface wetting, L – liquid phase, S – solid phase, G – gas phase; (b) partial GB wetting; (c) complete surface wetting; (d) complete GB wetting; (e) pseudopartial surface wetting; (f) pseudopartial GB wetting; (g) generic wetting phase diagram [70], PW – partial wetting, CW – complete wetting, PPW – pseudopartial wetting, CEP – critical end point, thick lines mark the discontinuous (first order) wetting transition, thin line mark the continuous (second order) wetting transition.

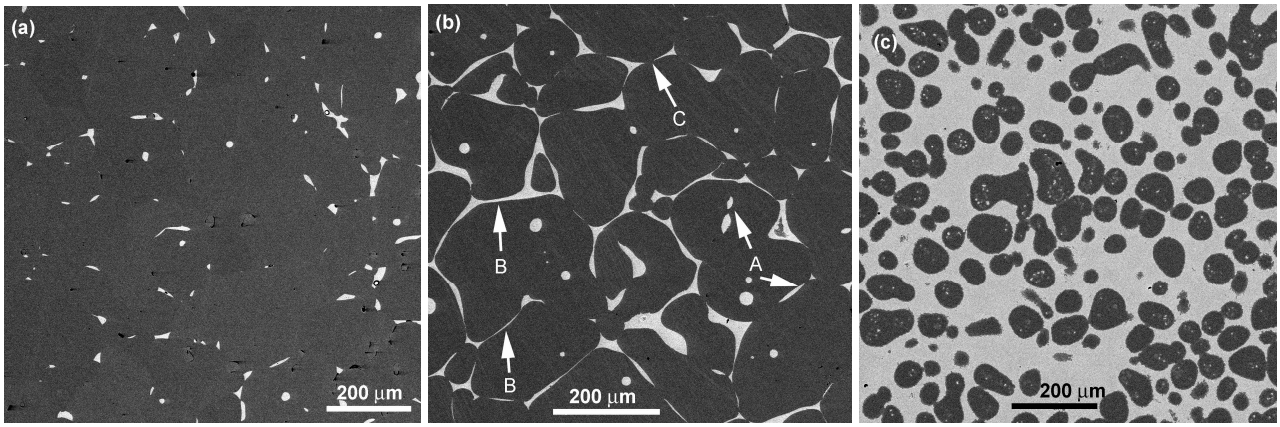

Fig. 2. The Cu – 22 wt.% In alloy annealed during 0.5 h in the (Cu)+liquid area of the Cu–In phase diagram. The Cu-based solid phase appears dark. The (solidified after quenching) In-rich liquid phase appears light. (a) 715°C, low amount of the melt, (b) 725°C, middle amount of the melt and (c) 745°C, big amount of the melt. **A:** (Cu) GBs incompletely wetted by the melt. **B:** (Cu) GBs completely wetted by the melt. **C:** (Cu) GB incompletely wetted by the melt, non-zero contact angle. However, the liquid layers from TJs almost meet in the middle of the Cu/Cu GB.

The correct experimental measurement of the contact angle θ is not an easy task. The most accurate measurement of a dihedral contact angle θ is possible in the experiments with bicrystals [26, 27]. In this case θ is measured in the section perpendicular to the flat individual GB and to the straight contact line between the GB and the liquid phase. In polycrystals the correct measurement of θ is much more complicated. If a GB contains lenticular liquid droplets, they are formed by two spherical solid/liquid interfaces. The correct θ value appears only in the section containing the common axis of both spherical solid/liquid interfaces. It can be measured either using transmission

electron microscopy (TEM) [28] or by careful three-dimensional analysis of the droplet shape [29, 30]. Moreover, the energy of GBs and interphase boundaries strongly depend on their misorientation and inclination parameters [31–33]. Therefore, also the θ values are different for different GBs in polycrystals. Even if all GBs would have the same energy and the same dihedral angle with the liquid phase, the conventional metallographic (or ceramographic, or petrographic) section would cross the lenticular particles in a random way. This would result in a certain scatter of measured θ values around the true values of the dihedral contact angle. If the amount of the liquid phase is large, melted layers would separate the solid grains even if the contact angle $\theta > 0°$ (compare the micrographs in Fig. 2 a to c). This phenomenon is called *apparently complete GB wetting* [34]. In the case of apparently complete GB wetting the liquid layers "meet each other" in a GB between TJs even by $\theta > 0°$ (see GB marked by the letter C in Fig. 2b and scheme in Fig. 3a). The apparently complete GB wetting phenomenon increases the percentage P_{app} of completely wetted GBs over and above the equilibrium value P_{equ}.

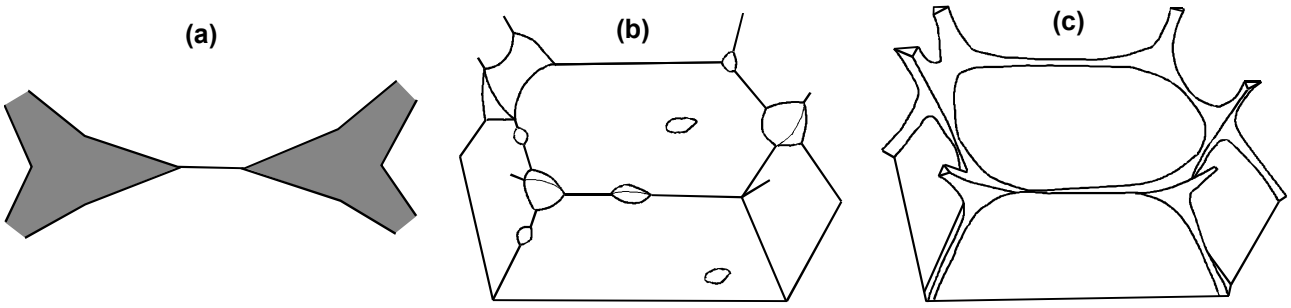

Fig. 3. (a) Scheme of the apparently complete GB wetting [35]. The liquid layers "meet each other" in a GB between TJs even by $\theta > 0°$. (b) Liquid droplets in GBs and TJs. (c) Liquid phase in GB triple junctions forms a continuous network of liquid channels [35].

Similar phenomenon is responsible for the formation of liquid channels along TJs. The dependence of microstructure of semi-solid polycrystals on the amount of liquid phase has been discussed for many years. Beere demonstrated that the gaseous or liquid phase in GB triple junctions forms a continuous network if its volume fraction is above a certain threshold value (see scheme in Fig. 3c) [35]. The threshold volume fraction varies with dihedral angle and increases with increasing θ [35, 36]. For example, for a dihedral angle of 15° already 2% of liquid phase is enough to connect all quadruple points by liquid channels (In a quadruple point four grains contact each other and three triple junctions cross). For the microstructure of liquid-phase sintered materials, a quantity known as the contiguity parameter has been defined [37, 38]. This is a quantitative measure of interphase contact, and is defined as the fraction of internal surface area of a phase shared with grains of the same phase in a two-phase microstructure. In liquid-phase sintering, these contacts serve a useful role in providing rigidity to a sintered compact, thereby controlling shape distortion. The contiguity depends strongly on the volume fraction of the solid phase and the dihedral angle; it increases with both parameters. At low dihedral angles, the contiguity increases rapidly as the volume fraction of the solid phase approaches unity [37]. Jurewicz and Watson defined the so-called equilibrium melt fraction which represents a minimum interfacial energy state when the melt is distributed uniformly along triple junctions in a partly-melted polycrystal [39]. The equilibrium melt fraction decreases with increasing θ. For example, it is only 2% for $\theta = 40°$ [39]. The θ value also influences the early stages of liquid-phase sintering when individual grains "swim" in a melt and form the first contact necks [40]. Similar observation were made also by investigations of ice melting and sintering of $ZnO–Bi_2O_3$ powders [3, 15, 41–43].

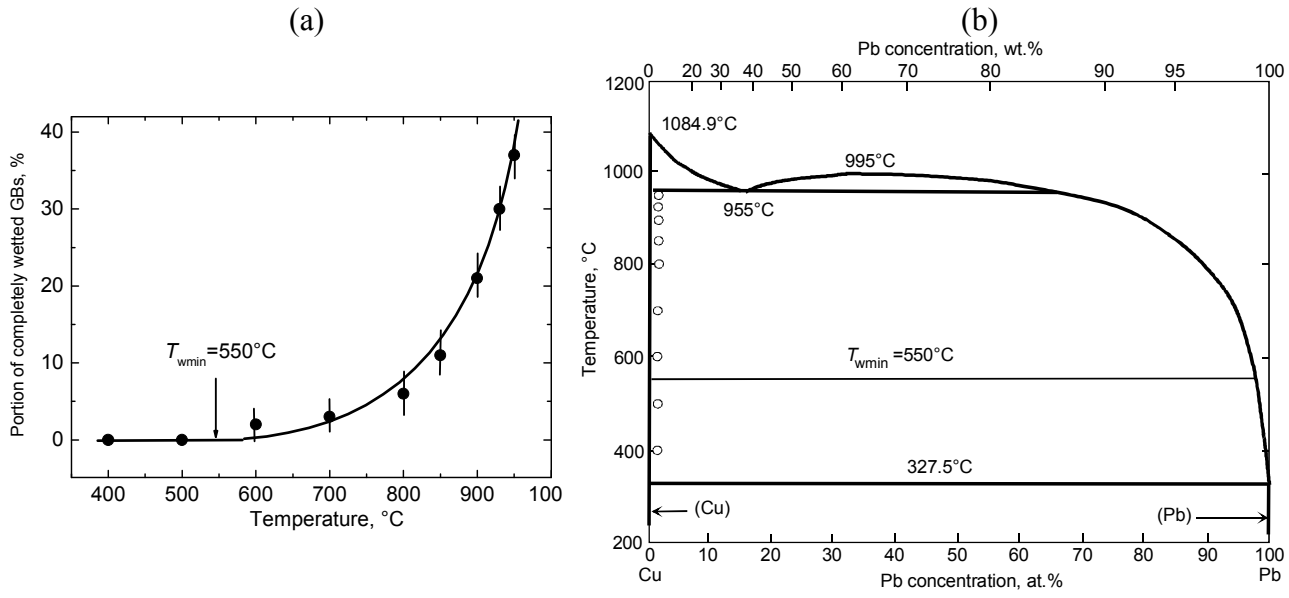

Fig. 4. (a) Temperature dependence of the portion of Cu GBs completely wetted by the Pb-rich melt. (b) Cu–Pb phase diagram with the tie-line of the T_{wmin} being the minimal temperature of the GB wetting transition. The experimental points are also shown.

The transition from incomplete to complete GB wetting proceeds at a certain T_w if the energy of two solid-liquid interfaces $2\sigma_{SL}$ becomes lower than the GB energy $\sigma_{GB} > 2\sigma_{SL}$. Cahn [44] and Ebner and Saam [45] first showed that the (reversible) transition from incomplete to complete wetting can proceed with increasing temperature, and that it is a true surface phase transformation. The GB wetting temperatures T_w, depend both on GB energy and solid-liquid interfacial energy which, in turn, depend on the crystallography of these interfaces [31, 46–48]. The transition from incomplete to complete GB wetting starts at a certain minimum temperature T_{wmin} which corresponds to the combination of maximum σ_{GB} and minimum σ_{SL}. The transition from incomplete to complete GB wetting finishes at a maximum temperature T_{wmax} which corresponds to the combination of minimum σ_{GB} and maximum σ_{SL}. The fraction of completely wetted GBs increases from 0 to 100% as the temperature increases from T_{wmin} to T_{wmax}. (Fig. 4a, Cu–Pb system and [49–55]). As a result, the new tie-lines appear in the S+L area of a phase diagram at T_{wmin} and T_{wmax} (Fig. 4b, Cu–Pb system [49–55]). Due to the simple geometric reasons, the wetting transition in TJs proceeds at T_{wTJ} which is below the T_{wmin} for GBs [56]. The wetting transition for the low-angle GBs proceeds at T_{wLA} which is above the T_{wmax} for high-angle GBs [33].

GBs can also be "wetted" by a second solid phase, the reversible transition from incomplete (Fig. 5b, GB marked by a letter **A**) to complete (Fig. 5b, GB marked by a letter **B**) solid phase wetting was observed for the first time in the Zn–Al system at a certain temperature T_{ws} [57]. The transition from incomplete to complete GB wetting by a liquid phase always proceeds with increasing temperature [49–55, 58]. It is easy to understand because the entropy of a liquid phase is higher than that of a solid one. Therefore, $2\sigma_{SL}$ has a good reason to decrease with increasing temperature steeper than σ_{GB}. In the first works on the GB wetting by a second solid phase the same tendency was observed [59, 60]. Namely, the (Zn)/(Zn) GBs became completely wetted by the (Al) solid phase with increasing temperature [59]. The (Al)/(Al) GBs also became completely wetted by the Al_3Mg_2 phase with increasing temperature [60]. However, there is no unambiguous reason for the GB wetting by a second solid phase, why the transition from incomplete (Fig. 5b, GB marked by a letter **A**) to complete (Fig. 5b, GB marked by a letter **B**) GB wetting cannot proceed by decreasing temperature. Recently we observed the GB wetting followed by the dewetting in the Co–Cu system [62]. This phenomenon occurs close to the Co Curie point, and it is known that if a paramagnet matrix becomes ferromagnetic, the additional attraction between grains may "squeeze"

the diamagnetic wetting phase from a GB. Similar transition from incomplete to complete GB wetting by a second solid phase can proceed by decreasing temperature also in "pure" case [63], without any additional phase transformations in a matrix like in [62]. In this case the temperature dependences of the GB energy σ_{GB} and energy of two solid-solid interfaces $2\sigma_{SS}$ also intersect at T_{ws} (Fig. 5a). However, in this case GB becomes completely wetted by a second solid phase below T_{ws} [63] and not above T_{ws} like in Refs. [58–61].

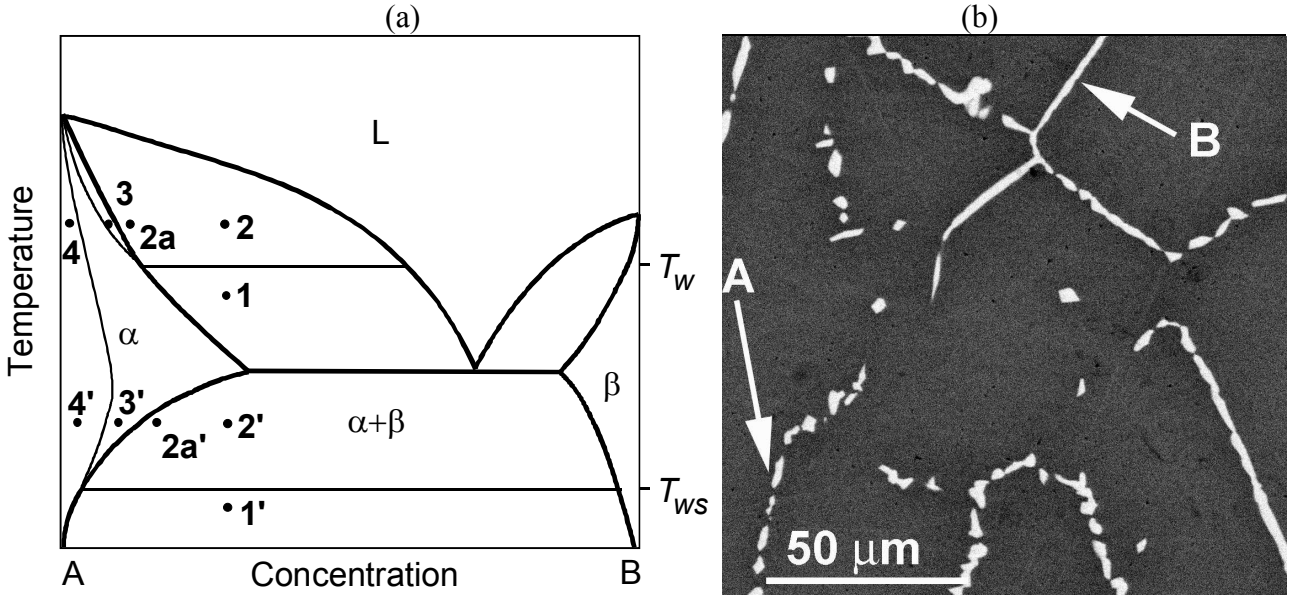

Fig. 5. (a) Schematic phase diagram with lines of GB phase transitions. T_W – temperature of the GB wetting phase transition (proceeds between points 1 and 2). T_{WS} – temperature of the GB solid phase wetting transition (proceeds between points 1' and 2'). Between points 3 and 4 the GB premelting phase transition occurs. Between points 3' and 4' the GB premelting phase transition occurs. In points 3 and 3' GB is covered by the equilibrium layer of a liquid-like or β-like phase which is unstable in the bulk. In points 2a and 2a' the wetting phase is in a deficit and cannot cover the GB with a thick layer. As a result GB is covered by the thin layer of a phase similar to that in points 3 and 3'.
(b) The Cu – 12 wt.% In alloy annealed at 430°C during 0.5 h in the (Cu) + δ (Cu_3In_7) two-phase area of the Cu–In phase diagram. The Cu-based solid solution appears dark. The δ (Cu_3In_7) phase appears light. **A:** (Cu) GBs incompletely wetted by the solid δ (Cu_3In_7) phase. **B:** (Cu) GBs completely wetted by the solid δ (Cu_3In_7) phase.

If the alloys are *slightly below the solidus line*, i.e. in the solid-solution area of the bulk phase diagram (marked as *3* in Fig. 5a), a thin layer of the liquid-like phase can be formed in GBs. In this area the liquid phase can appear in the GBs even though it is metastable in the bulk [16–18, 64]. This is because the system needs the additional energy ΔG for the formation of a metastable liquid phase. This energy can be compensated if the condition of full wetting, $\sigma_{GB} > 2\sigma_{SL}$, is fulfilled and the energy gain $\sigma_{GB} - 2\sigma_{SL}$ is higher than the energy loss ΔG. In this case a thin layer of a liquid-like phase may appear in the GB. The concentration of the second component in the liquid-like phase is also given by the liquidus line at the respective annealing temperature.

If the alloys are *deeply below the solidus line* in the solid-solution area of the bulk phase diagram (area *4* in Fig. 5a), ΔG further increases and $\sigma_{GB} - 2\sigma_{SL}$ cannot compensate ΔG any more. The liquid-like GB layer disappears below GB solidus line (dashed line in Fig. 5a). GB solidus begins at the melting point T_m of the pure component (in case of Al T_m = 662.5°C). GB solidus finishes at the intersection between GB wetting tie-line and bulk solidus. Each GB with its σ_{GB} has its own wetting tie-line and respective GB solidus. Only one (hypothetic) GB solidus line corresponding to maximal GB energy σ_{GBmax} and minimal $T_{w0\%}$ is drawn in Fig. 5a.

Such phenomenon is called prewetting or premelting. It has been first predicted by Cahn [44]. It can exist also if the second phase is solid. In the point *2′* (Fig. 5a) GB in the α-phase has to be substituted by the layer of β-phase and two α/β interphase boundaries (IBs). In the point *3′* GB is covered by the equilibrium layer of a β-like phase which is unstable in the bulk. In the points *4* and *4′* (Fig. 5a) GB is "pure" and contains only the usual segregation layer of component B.

In the case of complete wetting (Figs. 1c,d) $\sigma_{sg} > \sigma_{lg} + \sigma_{sl}$ or $\sigma_{gb} > 2\,\sigma_{sl}$, the contact angle is zero, and liquid spreads over the free surface or between grains. What happens, if the amount of liquid is small and surface (or GB) area is large? In this case the liquid spreads until both solid grains or solid and gas begin to interact with each other through the liquid layer. The liquid forms a "pancake" with a thickness e_s about 2-5 nm [8, 65]:

$$e_s = (A/4\pi S)^{1/2}, \quad (1)$$

where $S = \sigma_{sg} - \sigma_{sl} - \sigma_{lg}$ is the spreading coefficient on a strictly "dry" solid and A is the Hamaker constant [66]. In case of complete wetting $A > 0$ and $S > 0$ [65]. Such "pancake" on the free surface or between the grains is formed by the deficit of a wetting phase, i.e. in the α+L or α+β two-phase area of a phase diagram, but very close to the solidus or solvus line. This "pancake" is very similar to the prewetting or premelting thin films which form also very close to the solidus or solvus line, but on the other side of it, namely in the one-phase area α (points *2a* and *2a′*, scheme in Fig. 5a).

It has been shown that the transition from partial to complete wetting is the surface phase transformation [44, 45]. In the majority of cases the direct transition occurs from partial wetting (PW in the generic phase diagram Fig. 1g, proposed in Ref. 70) into complete wetting (CW), for example by increasing temperature [48, 52, 67] or decreasing pressure [68]. However, in some cases the state of pseudopartial wetting occurs (PPW in Fig. 1g) between partial and complete wetting. In this case the contact angle $\theta > 0$, the liquid droplet does not spread over the substrate, but the thin (few nm) precursor film exists around the droplet and separates substrate and gas (Fig. 1e). Such precursor film is very similar for the liquid "pancake" in case of complete wetting and deficit of the liquid phase (see above). This case is called pseudopartial wetting, it is possible when $A < 0$ and $S > 0$ [65]. In case of pseudopartial wetting the precursor exists together with liquid droplets, and in case of complete wetting the droplets disappear forming the "pancake".

The sequence of discontinous PW↔PPW and continuous PPW↔CW has been observed for the first time in the alcanes/water mixture [69]. The critical end point (CEP) was observed in a mixture of pentane and hexane which was deposited on an aqueous solution of glucose [70]. The first direct measurement of the contact angle in the intermediate wetting state (pseudo-partial wetting) was performed in the sequential-wetting scenario of hexane on salt brine [70]. Later the formation of Pb, Bi and binary Pb–Bi precursors surrounding liquid or solidified droplets has been observed on the surface of solid copper [71]. The pseudopartial wetting should in principle exist also for GBs (Fig. 1f).

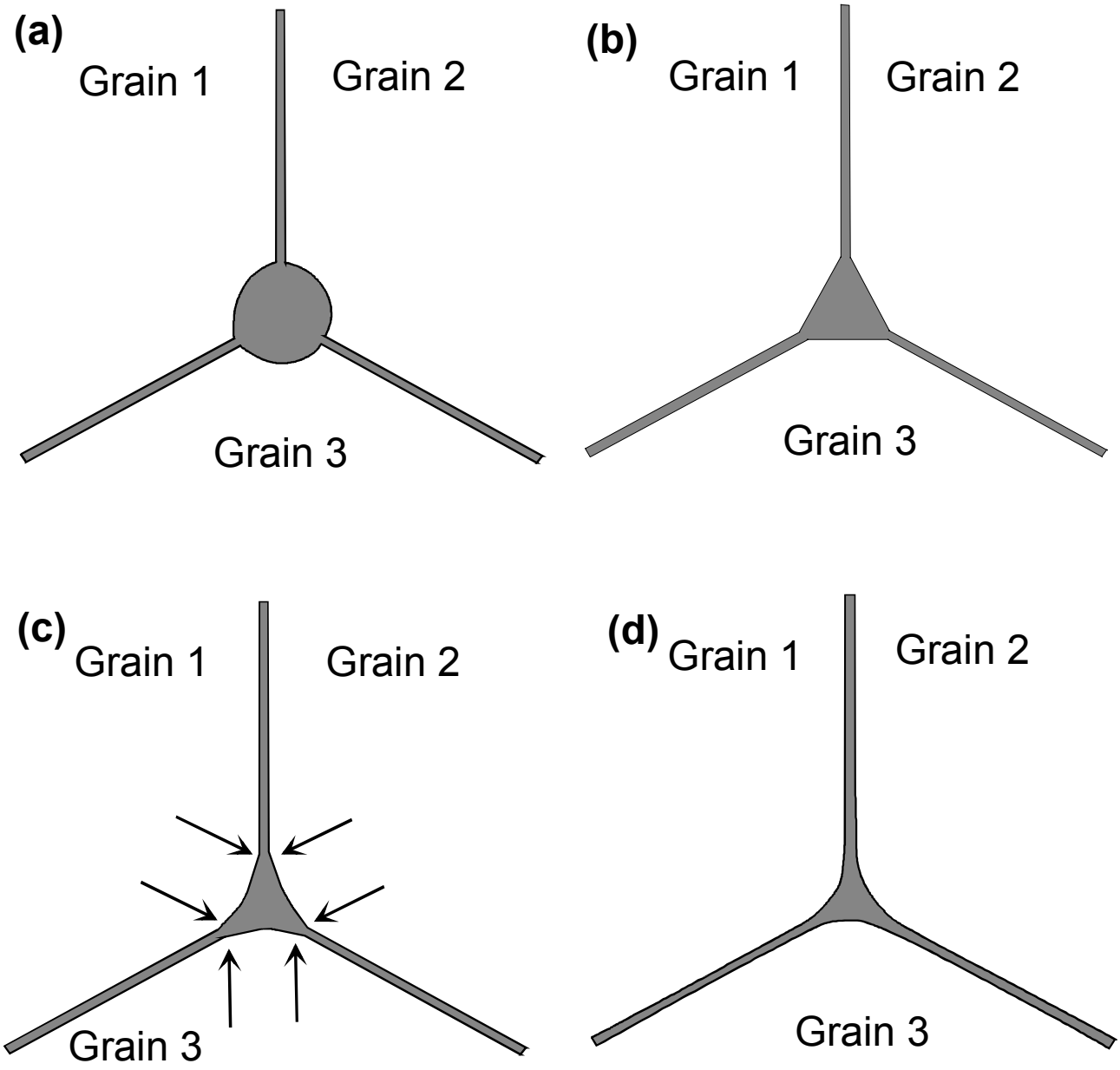

Fig. 6. Different configurations of liquid phase in the GB triple junction and thin quasi-liquid thin layers in the GB. (a) Pseudopartial GB wetting, $\theta > 60°$. (b) Pseudopartial GB wetting, $\theta = 60°$. (c) Pseudopartial GB wetting, $\theta < 60°$. The contact points between liquid phase in TJ and quasi-liquid layers in the GB are shown by arrows. (d) Complete GB wetting, $\theta = 0°$.

However, if one observes the thin GB layers of a constant thickness (or complexions), it is not easy to distinguish, whether one has the case of (1) prewetting/prewetting in the one-phase area of a bulk phase diagram; (2) thin GB "pancake" due to the deficit of wetting phase or (3) pseudopartial wetting by a liquid or solid phase. The big problem is that most frequently the bulk liquid or solid phase can be found only in the TJ "pockets". The pseudopartial wetting can be clearly identified only if the contact angle $\theta \geq 60°$ and the solid/liquid interface is convex (Figs. 6a,b) . If the contact angle $\theta < 60°$ and the solid/liquid interface is concave (Figs. 6c,d), the difference becomes very fine. If the solid/liquid interface has a discontinuity (two tangentials) between TJ pocket and GB layer (Figs. 6c), the pseudopartial wetting takes place. If the solid/liquid interface is continuous (one tangential) between TJ pocket and GB layer (Figs. 6d), the complete wetting with the deficit of wetting phase takes place. In the next sections we will discuss these possibilities for various systems.

Behavior of thin GB and TJ layers in various systems

Premelting/prewetting GB layers in metals. The GB premelting/prewetting phenomenon was observed for the first time by the investigations of zinc diffusion along the individual GBs in Fe–Si bicristals [26, 72–77]. Zn-based melt wets the GBs in all studied Fe-based alloys with 5, 10, 12.5 and 14 wt.% Zn. In the experiments the amount of liquid phase was chosen in such a way that it penetrated only to a certain depth. Below this depth the sample contained only one phase, namely the bcc-Fe with solved Zn. Close to the solubility limit (solvus) c_s of Zn in bcc-Fe the diffusivity of Zn atoms in GB was very high. The GB Zn diffusivity suddenly dropped to the conventional values at a certain concentration c_{bt}. The accelerated Zn GB diffusion has been explained by the formation of GB premelting/prewetting layer between c_s and c_{bt} [26, 72–77]. By increasing pressure the GB wetting disappears, the accelerated GB diffusion along the premelting/prewetting GB layer disappears as well [26, 76]. The $c_{bt}(T)$ premelting/prewetting lines have been constructed for the Fe-based alloys with 5, 10, 12.5 and 14 wt.% Zn [77]. The magnetic and/or chemical ordering in these alloys induces the additional attractive force between both grains, it leads to the disappearance of the GB premelting/prewetting together with accelerated GB zinc diffusion.

The GB wetting by liquid Ga in Al and Al-based alloys is very well known since it leads to the catastrophic failure of Al-parts [78]. The perfect wetting of Al-GBs in contact with the liquid Ga leads to the appearance of GB premelting/prewetting in the (Al) one-phase area of the Al–Ga phase diagram. The liquid-like GB layers form even at the very low Ga concentrations. In particular, the addition of only 10 or 50 ppm Ga to the high-purity Al accelerates the mobility of the same (individual) tilt GB measured in the conditions of a constant capillary driving force [79]. It is a quite unusual effect because the addition of an impurity always leads to the deceleration of GB migration. Only in case of the formation of a liquid-like layer, this GB layer could accelerate the GB migration.

Similar, to the Al–Ga system, the addition of very small amounts of Bi to Cu makes the Cu polycrystals extremely brittle. The surface of intergranular failure of the broken samples appears grey due to the segregated Bi layer. The intergranular brittleness permitted to break the Cu–Bi poly- and bicrystals in the Auger spectrometer and to measure the thickness of the Bi-enriched GB layers [80–86]. The samples with Bi content from 15 to 300 ppm were annealed between 400 and 1100°C, quenched and broken in the Auger spectrometer. It has to be underlined, that Bi-rich melt completely wets the majority of Cu GBs above 400°C. The Auger-measurements permitted to define the so-called GB solidus [81–83, 85]. It divides the one-phase solid solution (Cu) area of the phase diagram in two parts. Between the GB and bulk solidus lines the brittle failure “opens” the (Cu) GBs covered with about 2-4 monolayers (MLs) of Bi. This GB concentration does not depend on bulk Bi content and/or the annealing temperature. If one crosses the GB solidus, the GB concentration drops to the values below 1 ML and decreases with increasing temperature as the usual GB segregation has to do. The measurements on the annealed but not broken Cu–Bi samples show that the electrical conductivity suddenly increases when the network of Bi-rich layers isolating the copper grains one from another breaks [84]. The first (temperature) derivative of GB energy breaks at the GB solidus line. It means that the prewetting/premelting is the phase transition of first order. The measurements of the radio-tracer diffusion coefficients also shown that the Cu and Bi diffusivities suddenly increase by crossing the GB solidus line [87]. In other words, similar to the Fe–Si–Zn alloys, the liquid-like layer in GBs possesses the increased diffusivity.

Two independent groups observed that the ultra-fine-grained Al–Zn–Mg alloys demonstrate the extreme superplasticity (with elongation to failure up to 2500%) in the narrow temperature interval just below the bulk solidus [88–93]. This phenomenon appeared quite mysterious, especially because it disappeared by increasing content of Mg and/or Zn in the studied alloys. We investigated the binary Al–Zn and Al–Mg, as well as ternary Al–Zn–Mg alloys and found that the GB wetting phase transition takes place in these systems [19, 49, 51]. The position of T_{wmin} and T_{wmin} temperatures show where the GB solidus line should start at the bulk solidus lines. These estimations coincide with the temperatures and concentrations where the abnormally high superplasticity was observed in Refs. 88–93. The presence of liquid-like GB layers can explain why

the Al grains slide along the liquid, but very thin GBs without total failure of the material. Later we observed the thin Zn-rich layers in GBs and TJs of the Al–Zn samples quenched from the temperatures just below the bulk solidus line [16, 19, 94]. The DSC-measurements demonstrated that the fine grained Al–Zn alloys indeed start to melt about 10-15K below the bulk solidus line [19]. The solid Zn can also wet the GBs in Al. More over, the unusual superductility of the nanograined Al–Zn alloys as well as some DSC-indications show that the thin layers of Zn-rich phase can also exist in Al GBs close to the solvus line [19–22]

The thin layers of the liquid-like Ni-rich phase were recently observed in the W–Ni system [95, 96]. The technology for the liquid-phase and activated sintering was developed of alloys between W and Mo, on the one side, and Ni, Co, Fe, Cu, on the other side, in the end of 1940ies. It is based on the complete wetting of GBs in W and Mo by the liquid phase with lower melting temperature observed in experiments with poly- and bicrystals [95–101]. Since the accelerated sintering is observed not only in the two-phase area of the phase diagrams but also in the solid-solution area, one can suppose that the sintering is accelerated by the liquid-like GB layers like in Fe–Si–Zn or Cu–Bi systems. These liquid-like GB layers wee indeed found in the W–Ni system [95, 96].

The premelting phenomena on the surface and GBs were observed also in ice where they are extremely important and have big environmental consequences [2]. However, all these phenomena in the one-phase areas of the phase diagrams are connected with the complete GB wetting in the two-phase areas of the bulk phase diagrams and, therefore, do not need the concept of pseudopartial wetting for their explanation. Let us consider now the oxides, nitrides, borides, carbides etc.

Intergranular layers in zinc oxide. Zinc oxide is mainly used for manufacturing of varistors. Varistors exhibit highly non-linear current–voltage characteristics with a high resistivity below a threshold electric field, becoming conductive when this field is exceeded, enabling them to be used in current over-surge protection circuits [102]. The model usually proposed to account for the electrical properties of ZnO-based varistors is constituted on the basis of a bricklayer. ZnO-based varistors are approximated as a stacking of good conducting grains separated by grain boundaries, which support back-to-back double Schottky barriers [103–105]. Polycrystalline zinc oxide contains small amounts of dopants, mainly bismuth oxide. After liquid-phase sintering such material consists of ZnO grains separated by the Bi_2O_3-rich GB layers. Interfaces between the ZnO grains control the non-linear current-voltage characteristics. Though the Schottky barriers at ZnO/ZnO boundaries mainly control the voltage-dependent resistivity of a varistor, the Bi-rich GB phase also inputs into the overall resistivity.

The intergranular phase originates from the liquid-phase sintering. The sintering conditions alter the performances of ZnO varistors [104]. An increase in the sintering temperature results usually in a lowering in the nonlinearity of the current–voltage curve. Bhushan et al. pointed out that an increase in the sintering temperature would lower the Schottky barrier height [106] and Wong mentioned that the volatilization of Bi_2O_3 during the sintering would bring a loss in the non-ohmic property of the varistors [107]. The big amount of structural investigations permitted to construct the GB lines in the ZnO–Bi_2O_3 bulk phase diagram [5, 43, 108–115]. The first variant of the ZnO–Bi_2O_3 phase diagram has been experimentally constructed by Safronov et al. [116]. However, recently Guha et al. [117] found new γ-Bi_2O_3-phase and refined the ZnO–Bi_2O_3 phase diagram.

The liquid phase sintering of the ZnO+Bi_2O_3 mixture proceeds in the ZnO+liquid region of the ZnO–Bi_2O_3 phase diagram, i.e. above eutectic temperature of T_e = 738°C (usually at 850°C) [108]. During the liquid phase sintering, all ZnO/ZnO GBs are completely wetted by the thick layer of the melt. The thickness of the melt layer is governed only by the grain size and amount of the liquid phase (i.e. on the Bi_2O_3 content). At 850 °C liquid phase completely wets not only all ZnO/ZnO GBs, but also the free surface of the ZnO particles [5]. There is some indications that in the ZnO+liquid region close to T_e the complete GB wetting transforms into partial GB wetting (with contact angles above zero) [108]. In other words, in the ZnO–Bi_2O_3 phase diagram the GB wetting tie-line exists slightly above T_e.

The quenching from 850°C leaves a thick intergranular phase at the ZnO/ZnO GBs. However, the slow cooling below T_e leads to the dewetting of ZnO/ZnO GBs by crystallization of Bi_2O_3 [15, 109, 110]. Since the optimization of the varistor properties needs the slow cooling or a low-temperature post annealing, much work was devoted to the structure of GBs in varistors [15, 111, 112]. At the beginning of these investigations it was believed that all GBs contain thin Bi-rich intergranular phase. Then Clarke reported that most ZnO-GBs in a commercial varistor were free from the second-phase films, and the atomically abrupt GBs were observed using the lattice fringe imaging [118]. However, later Olsson et al. found the continuous Bi-rich films in the majority of ZnO/ZnO GBs, and only a few GBs were atomically ordered up to the GB plane [113,114]. It was also found that the treatment at high hydrostatic pressure of 1 GPa leads to the desegregation of ZnO/ZnO GBs [115]. During desegregation the Bi-rich GB phase disappears due to the Bi GB diffusion towards the secondary phase in the GB triple junctions.

Wang and Chiang studied the ZnO with 0.23 mol. % at Bi_2O_3 700°C [108]. The samples were brought into equilibrium at this temperature from three different starting points: (a) after liquid phase sintering at 850 °C followed by 24 h annealing at 700°C and slow cooling down to the room temperature; (b) by sintering directly at 700°C (i.e. below T_e, without presence of any liquid phase) for 2 h by 1 GPa followed by the annealing at 700°C at the room pressure; (c) equilibrium segregation at 700°C was reached from the high-pressure desegregated state. Wang and Chiang discovered that in all three cases the equilibrium GB state at 700°C is the amorphous intergranular film of 1.0–1.5 nm in thickness. In other words, a thin intergranular film has a lower free energy in comparison with pure crystal-crystal GB. The thermodynamic conditions for the existence of such films were studied by Clarke [7]. After desegregation at high temperature, GBs are free from any Bi-rich layers (thin or thick). Crystalline Bi_2O_3 particles are present in the GB triple junctions. However, after additional annealing at the same temperature of 700°C but at atmospheric pressure, Bi diffuses back from the triple junctions into the GBs forming the amorphous GBs films of 1.0–1.5 nm in thickness. In other words, the amorphous films builds not from the undercooled liquid, but in the solid phase, as a result of Bi GB diffusion. Moreover, the thin amorphous film covers not only the ZnO/ZnO GBs, but also the intrephase boundary between ZnO grains and Bi_2O_3 particle in the ZnO GB triple junction.

This behaviour can be explained by the *pseudopartial wetting* [5, 65]. At certain thermodynamic conditions liquid droplets have a non-zero contact angle with a solid substrate (or a GB), but the rest of a substrate surface (or a GB) is not dry, but covered by a thin film of few nm thickness. For example, the liquid Bi-rich nanodroplets (5–15 nm) with contact angle of about 40° were observed on the top of the amorphous film of 1.95 nm thickness on the ZnO surface facets [5]. In ZnO–Bi_2O_3 samples studied in Ref. [119] can be clearly seen that the amorphous Bi-rich thin GB layer has the non-zero contact angle with the Bi_2O_3 phase in TJs. This situation corresponds to scheme in Fig. 6c and not to that in Fig.6d. In other words, the *pseudopartial GB wetting* has been observed in Ref. [119]. Most probably, the pseudopartial GB wetting ZnO–Bi_2O_3 system is observed not in all GBs and not in all conditions. For example, the TJs in Ref [120, 121] clearly correspond to the scheme Fig. 6d (complete wetting, $\theta = 0°$)

Intergranular layers in conducting oxides of fluorite structure. Conducting oxides of fluorite structure have received much attention in recent years due to their ionic conductivity with the applications as electrolytes for the solid oxide fuel cells (SOFC) and oxygen sensors. Yttria-stabilized zirconia (YSZ) is by far the most widely used solid electrolyte for technological applications. The main factors driving the interest for this solid electrolyte are its high chemical stability in oxidizing or reducing environments and its compatibility with a variety of adjoining electrode materials. It is presently employed at temperatures above 600 °C. Other oxides like calcia or scandia can also be used for stabilization of zirconia. Though stabilized zirconia exhibits good conductivity at high temperatures, however, the need for a better oxygen-conducting material in SOFCs has shifted interest to doped ceria [122], which exhibits good conductivity at lower temperatures. Usual doping ions for CeO_2 are Gd^{3+}, Sm^3+ and Y^3+. Substitution of the Ce^{4+} cations in the lattice results in the formation of vacancies and enhances the ionic conductivity.

GB wetting phases. It has been shown that the maximum of the ionic conductivity of yttria-stabilized zirconia occurs around 9.5 mol% Y_2O_3 [123]. Measurements of conductivity and oxygen diffusivity confirmed that YSZ are the ionic conductors at the temperatures as low as 200 °C [124]. Critical for the low-temperature applications are the internal interface properties of YSZ. In YSZ a glassy phase was frequently observed in GBs and GB triple junctions. In Ref. 125 two YSZs (called Z_C and Z_F) were sintered from powders prepared through two different processing routes. In samples Z_C the glassy phase wetted GBs and GB triple junctions. Glassy phase in triple junctions has a shape of stars with zero contact angles at GBs. These „stars" continue towards GBs as GB wetting layers. In samples Z_F the amorphous precipitates of glassy phase in triple junctions are lenticular, and spherical glass pockets are widely dispersed in the bulk of grains, but there is no evidence of glassy films at grain boundaries. As a result, the grain boundary conductivity of the Z_F polycrystal, which shows glass-free grain boundaries, is about 3 orders of magnitude higher than that of the Z_C material. These results are consistent with the mechanism of oxygen-ion transport across grain boundaries suggested by Badwal [126]. Conductivity occurs without any constriction of current pathways in the Z_F ceramics, while it is restricted to the unwetted grain boundaries in the Z_C ceramics. Therefore, if a GB wetting phase is detrimental, one can change a composition in such a way, that the GB wetting conditions are not fulfilled any more. In this case the GB network of detrimental phase is broken and properties of a material improve. Thus, changing GB wetting conditions by microalloing one can improve the properties of a conducting oxide.

Monolayer GB segregation. Even in the absence of the GB layers of wetting phases, the properties of conducting oxides can be controlled by the conventional (less that one monolayer) GB segregation. In the zirconia obtained by the conventional sintering methods a minor amount of silicon, originated from contaminated starting materials, detrimentally influences the conductivity of fuel cells oxides [127]. This effect originates from silicon coverage of GBs in stabilized zirconia with formation of a continuous GB network in the polycrystal. Silicon-containing phase form lenticular GB particles and they do not wet the GBs. However, if the Si concentration in GBs reaches about 0.5 monolayer, the GB conductivity drastically decreases, and does not change much with further increase of GB Si content [127]. However, if the grain size in stabilized zirconia decreases from micrometer into the nanometre range, the amount of silicon is not more enough to contaminate all GBs. As a result, the specific GB conductivities in nanocrystalline calcia-stabilized zirconia increase about 5 times [127]. The specific GB conductivities of the nanocrystalline YSZ samples (grain size 40 nm) is 1–2 orders of magnitude higher than that of the microcrystalline samples (grain size 400-1000 nm) [128]. Therefore, the detrimental effect of Si-contamination vanishes and overall properties of nanostructured zirconia improve. Similar effect of grain size was observed in the scandia-stabilized zirconia [129]. The specific GB conductivities measured using the impedance spectroscopy increase almost two orders of magnitude when grain size decreases from 6000 to 60 nm. It is an important example, how the GB engineering (tailoring the polycrystal properties by controlling the GB structure and composition) can improve the properties of nanostructured oxides for fuel cells. Thus, decreasing the grain size, one can dilute the detrimental GB segregation down to the harmless value and improve the properties of a conducting oxide.

Scavengers for GB impurities. Another way to compensate the detrimental Si influence and to improve the GB conductivity in zirconia and ceria is to use the so-called scavengers. It has been shown already in 1982 that small additions of Al_2O_3 drastically improve the ionic conductivity of YSZ [130]. Later Al_2O_3 was identified as a most effective dopant in increasing the GB conductivity of zirconia-based electrolytes [131–134]. Butler and Drennan suggested that alumina acts as a „scavenger" for SiO_2 since the affinity of SiO_2 to Al_2O_3 is greater than to the ZrO_2 [130]. As a result the particles of Al_2O_3 present in the ceramic „sweep out" silicon from zirconia GBs. It results in the purification effect similar to that of the decrease of grain size. The best scavenger for ceria-based electrolyte is the iron oxide [135].

Heavy doping. Heavy doping is another way to change the GB composition and, therefore, improve the conductivity of an oxide. Cerium oxide is a mixed ionic/electronic conductor and exhibits high ionic conductivity when doped with lower valent cations (acceptors). As the oxygen

vacancy mobility is even higher than in cubic zirconia—the other prominent fluorite-structured oxygen ion conductor—there has been considerable interest in the potential of ceria-based solid electrolytes for applications in solid oxide fuel cells or oxygen membranes. In Ref. 136 the microcrystalline ceria was doped with Y, La and Gd in the broad concentration range between 0.1 and 27 at. %. The grain boundary effect, which is indicated by the gap between the bulk and the total conductivity, was found to decrease rapidly as the acceptor concentration increases. The GB conductivity drastically increases at the acceptor concentration between 2 and 10 at.%. Simple estimation reveals that the GB conductivity reaches the bulk value when all GBs become covered with a monolayer of an acceptor impurity (for the ceria grain size of about 1 μm). The ZrO_2 TJs with continuous transition to the GB thin film (like in the scheme Fig 6d) has been observed in Ref. 137.

Intergranular layers in perovskites. Perovskite-type oxides ($BaTiO_3$, $SrTiO_3$, $LaAlO_3$, $LaCrO_3$, etc.) have recently attracted considerable attention for their applications in high-temperature electrochemical devices, such as electrolytes and electrodes of solid oxide fuel cells, oxygen permeating membranes and sensors etc. For the ionic conduction, some perovskites exhibit surprisingly high ionic conductivities, higher than those of well-known zirconia-based materials. The impedance spectroscopy permits to separate bulk and GB inputs in overall conductivity. In many cases the overall conductivity of perovskites is determined by the grain boundary resistance, like for example that of Sr and Mg doped $LaAlO_3$ below 550 °C [138]. However, the GB input into overall conductivity gradually decreases by increasing temperature. GBs in perovskites mainly contain the conventional GB segregation layer. Only in few cases (like in $BaTiO_3$ sintered from powder particles with Mn coating) the GB amorphous region with a width of about 1 nm was observed [139]. The boundary width in such polycrystals is about five times larger than that in the $BaTiO_3$ sintered from powder particles without Mn coating. The electrostatic potential barrier height of the $BaTiO_3$ ceramics increased from 0.18 to 0.24 eV, due to the increase in the width of the excess negative charge layer from 70 to 120 nm, with increasing the amount of the powder coating material from 0 to 1.0 at.%. A systematic variation of the grain boundary features with the amount of coating material indicates the possibility of using this synthesis method to get fine control over the chemistry and electrical properties of the semiconducting $BaTiO_3$ ceramics.

Intergranular layers in alumina. The observation of thin GB layers in Al_2O_3 permitted S.J. Dillon, M. Tang, W. Craig Carter and M.P. Harmer [12] to introduce the term “complexions” to describe the general phenomenon of thin GB films. The observed amorphous GB thin films (called also IGFs [10]) are of very uniform thickness, however, the thickness can be different for different GBs [12, 13, 140, 141]. Moreover, the transition between IGFs (complexions) of different thickness is possible [12, 13, 141]. Very interesting are also the amorphous films of uniform thickness observed in the interphase boundaries between sapphire and metals [142, 143]. Both IGFs corresponding to the complete wetting with $\theta = 0°$ (case shown in Fig 6d) and to the pseudopartial wetting with $\theta > 0°$ (case shown in Fig 6c) can be observed in sintered alumina depending on sintering additives [144]. Unfortunately, to the best of our knowledge, all published micrographs do not allow to distinguish whether these

Intergranular layers in nitrides. Silicon nitride Si_3N_4 is a very important structural material for high-temperature applications [145 and references therein]. As many high-temperature materials, it is produced with the aid of liquid-phase sintering. SiO_2 and other additions are used to form the low-melting phase permitting to sinter the Si_3N_4 powder particles with high melting point. Already in 1980ies it has been observed that after sintering and cooling the solidified liquid phase remains in the TJ “pockets” and forms the very thin (2-4 nm) GB amorphous layers of very constant thickness [146]. David R. Clarke proposed in his seminal work [7] the idea coming back to the work of Cahn [44] that these films are thermodynamically stabilized by a certain combination of attractive and repulsive forces. Afterwards these films were in details studied both experimentally and

theoretically [4–13, 147–161]. The composition of amorphous GB thin films (IGFs [10]) usually differs from that of the phase in TJ "pockets" [145 and references therein], the coincidence GBs with low energy do not contain the IGFs [147], the thickness of IGFs depends on their composition (i.e. on the presence of various sintering additives like CaO [148], F [149, 150], SiO_2 [151–154], La_2O_3, Sm_2O_3, Er_2O_3, Yb_2O_3, and Lu_2O_3 [155], La_2O_3 [156], La_2O_3 and Lu_2O_3 [157], Lu, Si, Mg [158], La_2O_3 [159], La_2O_3–MgO [160]).

In this review the question is interesting for us, whether these IGF correspond to the complete wetting with deficit of a wetting phase, with $\theta = 0°$ (case shown in Fig 6d) or to the pseudopartial wetting with $\theta > 0°$ (case shown in Fig 6c). To the best of our knowledge, in all published micrographs only the second phase in TJ "pockets" is present, and no lenticular particles in GBs are visible [7, 145, 148, 153–158, 161]. Moreover, the TJ "pockets" with $\theta > 60°$ (case shown in Fig 6a) are absent. In most cases the perfect complete wetting with $\theta = 0°$ (like in Fig 6d) can be observed [150, 154, 160]. Only in few cases, in some contacts of phase in TJ "pockets" and IGFs the shape discontinuity of the interphase boundary Si_3N_4/(sintering phase) can be observed (Si_3N_4 with 5 wt. % CeO_2 and 1 wt. % Al_2O_3 [161], Al_2O_3 and Al_2O_3 [7, 145], 2 wt. % Y_2O_3 [154]).

Conclusions

The thin intergranular films of a second phase are observed in the last decade in metals, oxides, nitrides etc. Especially frequently they appear as a result of liquid phase sintering. Thin intergranular films can be either detrimental or beneficial. In any case they drastically change the properties of Gbs and of a polycrystal as whole. If they resulted from complete GB wetting by a second (liquid or solid) phase, they can form only in a narrow neighbourhood of a soliudus or solvus lines in the bulk phase diagrams. However, the phenomenon of pseudopartial wetting has been recently predicted and then found (first in the liquid mixtures and then on the solid surfaces). In case of pseudopartial wetting the thin intergranular films can exist in the equilibrium with lenticular GB particles of a second phase. In other words, the thin intergranular films can exist in broad two-phase regions of phase diagrams and could be very useful for various applications.

Acknowledgements

This work was supported by the Russian Foundation of Basic Research (contract 10-02-00086), Erasmus Mundus programme of EU and the grant of President of Russian Federation for young scientists (MK-3748.2011.8) for the financial support.

References

[1] B.B. Straumal, A.A. Mazilkin, S.G. Protasova, A.A. Myatiev, P.B. Straumal, G. Schütz, P.A. van Aken, E. Goering, B. Baretzky: Phys. Rev. B Vol. 79 (2009), p. 205206.
[2] B. Zhao, G. Gottstein, L.S. Shvindlerman: Acta Mater. Vol. 59 (2011), p. 623.
[3] J.G. Dash, H. Fu, J.S. Wettlaufer: Rep. Prog. Phys. Vol. 58 (1995), p. 115.
[4] P. Bueno, J. Varela, E. Longo: J. Eur. Ceram. Soc. Vol. 28 (2008), p. 505.
[5] J. Luo, Y.M. Chiang, R.M. Cannon: Langmuir Vol. 21 (2005), p. 7358.
[6] J. Luo, M. Tang, R. Cannon, C.W. Carter, Y.M. Chiang: Mater. Sci. Eng. A Vol. 422 (2006), p. 19.
[7] D.R. Clarke: J. Am. Ceram. Soc. Vol. 70 (1987), p. 15.
[8] J. Luo: Crit. Rev. Solid State Mater. Sci. Vol. 32 (2007), p. 67.
[9] J. Luo, Y.M. Chiang: Ann. Rev. Mater. Res. Vol. 38 (2008), p. 227.
[10] A. Subramaniam, C. Koch, R.M. Cannon, M. Rühle: Mater. Sci. Eng. A Vol. 422 (2006), p. 3.
[11] I. Maclaren: Ultramicroscopy Vol. 99 (2004), p. 103.
[12] S.J. Dillon, M. Tang, W. Craig Carter, M.P. Harmer: Acta. Mater. Vol. 55 (2007), p. 6208.
[13] M.P. Harmer: J. Am. Ceram. Soc. Vol. 93 (2010), p. 301.

[14] B.B. Straumal, S.G. Protasova, A.A. Mazilkin, A.A. Myatiev, P.B. Straumal, G. Schütz, E. Goering, B. Baretzky: J. Appl. Phys. Vol. 108 (2010), p. 073923.
[15] B.B. Straumal, A.A. Myatiev, P.B. Straumal, A.A. Mazilkin, S.G. Protasova, E. Goering, B. Baretzky: JETP Letters Vol. 92 (2010), p. 396.
[16] B.B. Straumal, A.A. Mazilkin, O.A. Kogtenkova, S.G. Protasova, B. Baretzky: Phil. Mag. Lett. Vol. 87 (2007), p. 423.
[17] B. Straumal, R. Valiev, O. Kogtenkova, P. Zieba, T. Czeppe, E. Bielanska, M. Faryna: Acta Mater. Vol. 56 (2008), p. 6123.
[18] O.A. Kogtenkova, B.B. Straumal, S.G. Protasova, A.S. Gornakova, P. Zięba, T. Czeppe: JETP Lett. Vol. 96 (2012), p. 380.
[19] R.Z. Valiev, M.Yu. Murashkin, B.B. Straumal: Mater. Sci. Forum Vols. 633-634 (2009), p. 321.
[20] R.Z. Valiev, M.Y. Murashkin, A. Kilmametov, B.B. Straumal, N.Q. Chinh, T.G. Langdon: J. Mater. Sci. Vol. 45 (2010), p. 4718.
[21] N.Q. Chinh, T. Csanádi, J. Gubicza, R.Z. Valiev, B.B. Straumal, T.G. Langdon: Mater Sci Forum Vols. 667-669 (2011), p. 677.
[22] N.Q. Chinh, T. Csanádi, T. Győri, R.Z. Valiev, B.B. Straumal, M. Kawasaki, T.G. Langdon: Mater. Sci. Eng. A Vol. 543 (2012), p. 117.
[23] R.M. German, P. Suri, S.J. Park: J. Mater. Sci. Vol. 44 (2009), p. 1.
[24] E.B. Watson: Geology Vol. 10 (1982), p. 236.
[25] D. Laporte, E.B. Watson: Chem. Geol. Vol. 124 (1995), p. 161.
[26] B.B. Straumal, W. Gust: Mater. Sci. Forum Vol. 207 (1996), p. 59.
[27] B.B. Straumal, W. Gust, T. Watanabe: Mater. Sci. Forum Vol. 294 (1999), p. 411.
[28] H. Gabrisch, U. Dahmen, E. Johnson: Microsc. Res. Techn. Vol. 42 (1998), p. 241.
[29] L. Felberbaum, A. Rossoll, A. Mortensen: J. Mater. Sci. Vol. 40 (2005), p. 3121.
[30] D. Empl, L. Felberbaum, V. Laporte, D. Chatain, A. Mortensen: Acta Mater. Vol. 57 (2009), p. 2527.
[31] B.B. Straumal, L.M. Klinger, L.S. Shvindlerman: Acta metall. Vol. 32 (1984), p. 1355.
[32] B.B. Straumal, L.S. Shvindlerman: Acta metall. Vol. 33 (1985), p. 1735.
[33] B.B. Straumal, B.S. Bokstein, A.B. Straumal, A.L. Petelin: JETP Letters Vol. 88 (2008), p. 537.
[34] A.B. Straumal, B.S. Bokstein, A.L. Petelin, B.B. Straumal, B. Baretzky, A.O. Rodin, A.N. Nekrasov: J. Mater. Sci. Vol. 47 (2012), p. 8336.
[35] W. Beere: Acta. Metall. Vol. 23 (1975), p. 131.
[36] J.R. Bulau, H.S. Waff, J.A. Tyburczy: J. Geophys. Res. Vol. 84 (1979), p. 6102.
[37] R.M. German: Metal. Trans. A Vol. 16 (1985), p. 1247.
[38] Y. Takei: J. Geophys. Res. B Vol. 8 (1998), p. 18183.
[39] S.R. Jurewicz, E.B. Watson: Geochim. Cosmochim. Acta Vol. 49 (1985), p. 1109.
[40] J. Liu, R.M. German: Metal. Mater. Trans. A Vol. 32 (2001), p. 165.
[41] J.F. Nye: J. Glaciol. Vol. 35 (1989), p. 17.
[42] J.F. Nye. In: N. Maeno, T. Hondoh (eds): *Physics and Chemistry of Ice* (Kokhido University Press, Sapporo, 1992), p. 200.
[43] H. Mader: J. Glaciol. Vol. 38 (1992), p. 333.
[44] J.W. Cahn: J. Chem. Phys. Vol. 66 (1977), p. 3667.
[45] C. Ebner, W.F. Saam: Phys. Rev. Lett. Vol. 38 (1977), p. 1486.
[46] B.B. Straumal, S.A. Polyakov, E.J. Mittemeijer: Acta Mater. Vol. 54 (2006), p. 167.
[47] J. Schölhammer, B. Baretzky, W. Gust, E. Mittemeijer, B. Straumal: Interf. Sci. Vol. 9 (2001), p. 43.
[48] B. Straumal, T. Muschik, W. Gust, B. Predel: Acta metal. Mater. Vol. 40 (1992), p. 939.
[49] B. Straumal. G. López, W. Gust, E. Mittemeijer. In: M.J. Zehetbauer and R.Z. Valiev. (eds.) *Nanomaterials by severe plastic deformation. Fundamentals – Processing – Applications*, (J.Wiley VCH Weinheim, Germany, 2004), p. 642.

[50] C.-H. Yeh, L.-S. Chang, B.B. Straumal: J. Phase Equilbria & Diff. Vol. 30 (2009), p. 254.
[51] B.B. Straumal, G. López, E. J. Mittemeijer, W. Gust, A.P. Zhilyaev: Def. Diff. Forum Vols. 216-217 (2003), p. 307.
[52] B.B. Straumal, A.S. Gornakova, O.A. Kogtenkova, S.G. Protasova, V.G. Sursaeva, B. Baretzky: Phys. Rev. B Vol. 78 (2008), p. 054202.
[53] V. Murashov, B. Straumal, P. Protsenko: Def. Diff. Forum Vol. 249 (2006), p. 235.
[54] C.-H. Yeh, L.-S. Chang, B. B. Straumal: Def. Diff. Forum Vols. 258–260 (2006), p. 491.
[55] B. Straumal, D. Molodov, W. Gust: Interface Sci. Vol. 3 (1995), p. 127.
[56] B.B. Straumal, O. Kogtenkova, P. Zięba: Acta Mater. Vol. 56 (2008), p. 925.
[57] G.A. López, E.J. Mittemeijer, B.B. Straumal: Acta Mater. Vol. 52 (2004), p. 4537.
[58] N. Eustathopoulos: Int. Met. Rev. Vol. 28 (1983), p. 189.
[59] G.A. López, E.J. Mittemeijer, B.B. Straumal:Acta Mater. Vol. 52 (2004), p. 4537.
[60] B.B. Straumal, B. Baretzky, O.A. Kogtenkova, A.B. Straumal, A.S. Sidorenko: J. Mater. Sci. Vol. 45 (2010), p. 2057.
[61] A.S. Gornakova, B.B. Straumal, A.L. Petelin, A.B. Straumal: Bull. Russ. Ac. Sci.: Phys. Vol. 76 (2012), p. 102.
[62] B.B. Straumal, O.A. Kogtenkova, A.B. Straumal, Yu.O. Kuchyeyev, B. Baretzky: J. Mater. Sci. Vol. 45 (2010), p. 4271.
[63] S.G. Protasova, O.A. Kogtenkova, B.B. Straumal, P. Zięba, B. Baretzky: J. Mater. Sci. Vol. 46 (2011), p. 4349.
[64] B.B. Straumal, B. Baretzky: Interf. Sci. Vol. 12 (2004), p. 147.
[65] F. Brochard-Wyart, J.M. di Meglio, D. Quéré, P.G. de Gennes: Langmuir Vol. 7 (1991), p. 335.
[66] B.B. Straumal, P. Zieba, W. Gust: Int. J. Inorg. Mater. Vol. 3 (2001), p. 1113.
[67] C. Ebner, W.F. Saam: Phys. Rev. Lett. Vol. 38 (1977), p. 1486.
[68] B. Straumal, E. Rabkin, W. Lojkowski, W. Gust, L.S. Shvindlerman: Acta mater. Vol. 45 (1997), p. 1931.
[69] E. Bertrand, H. Dobbs, D. Broseta, J. Indekeu, D. Bonn, J. Meunier: Phys. Rev. Lett. Vol. 85 (2000), p. 1282.
[70] S. Rafaï, D. Bonn, E. Bertrand, J. Meunier: Phys. Rev. Lett. Vol. 92 (2004), p. 245701.
[71] J. Moon, S. Garoff, P. Wynblatt, R. Suter: Langmuir Vol. 20 (2004), p. 402.
[72] E.I. Rabkin, V.N. Semenov, L.S. Shvindlerman, B.B. Straumal: Acta metall. mater. Vol. 39 (1991), p. 627.
[73] O.I. Noskovich, E.I. Rabkin, V.N. Semenov, B.B. Straumal, L.S. Shvindlerman: Acta metall. mater. Vol. 39 (1991), p. 3091.
[74] B.B. Straumal, O.I. Noskovich, V.N. Semenov, L.S. Shvindlerman, W. Gust, B. Predel: Acta metall. mater. Vol. 40 (1992), p. 795.
[75] E. Rabkin, B. Straumal, W. Gust: Z. Metallk. Vol. 87 (1996), p. 948.
[76] B. Straumal, E. Rabkin, W. Lojkowski, W. Gust, L.S. Shvindlerman: Acta mater. Vol. 45 (1997), p. 1931.
[77] B. Straumal, E. Rabkin, L. Shvindlerman, W. Gust: Mater. Sci. Forum Vols. 126–128 (1993), p. 391.
[78] B. Straumal, S. Risser, V. Sursaeva, B. Chenal, W. Gust: J. Physique IV Vol. 5-C7 (1995), p. 233.
[79] D.A. Molodov, U. Czubayko, G. Gottstein, L.S. Shvindlerman, B.B. Straumal, W. Gust: Phil. Mag. Lett. Vol. 72 (1995), p. 361.
[80] L.-S. Chang, B. B. Straumal, E. Rabkin, W. Gust, F. Sommer: J. Phase Equl. Vol. 18 (1997), p. 128.
[81] L.-S. Chang, E. Rabkin, B. Straumal, P. Lejcek, S. Hofmann, W. Gust: Scripta mater. Vol. 37 (1997), p. 729.
[82] L.-S. Chang, E. Rabkin, B. B. Straumal, S. Hoffmann, B. Baretzky, W. Gust: Defect Diff. Forum Vol. 156 (1998), p. 135.

[83] L.-S. Chang, E. Rabkin, B.B. Straumal, B. Baretzky, W. Gust: Acta mater. Vol. 47 (1999), p. 4041.
[84] B. Straumal, N. E. Sluchanko, W. Gust: Def. Diff. Forum Vols. 188-190 (2001), p. 185.
[85] B. Straumal, S. I. Prokofjev, L.-S. Chang, N. E. Sluchanko, B. Baretzky, W. Gust, E. Mittemeijer. Def. Diff. Forum Vols. 194-199 (2001), p. 1343.
[86] J. Schölhammer, B. Baretzky, W. Gust, E. Mittemeijer, B. Straumal: Interf. Sci. Vol. 9 (2001), p. 43.
[87] S.V. Divinski, M. Lohmann, Chr. Herzig, B. Straumal, B. Baretzky, W. Gust: Phys. Rev. B Vol. 71 (2005), p. 104104.
[88] K. Higashi, T.G. Nieh, M. Mabuchi, J. Wadsworth: Scripta Metall. Mater. Vol. 32 (1995), p. 1079.
[89] Y. Takayama, T. Tozawa, H. Kato: Acta Mater. Vol. 47 (1999), p. 1263.
[90] M. Mabuchi, K. Higashi, Y. Okada, S. Tanimura, T. Imai, K. Kubo: Scripta. Metall. 25 (1991) 2003.
[91] K. Higashi, Y. Okada, T. Mukai, S. Tanimura: Scripta Metall. Vol. 25 (1991), p. 2053.
[92] H. Iwasaki, T. Mori, M. Mabuchi, K. Higashi: Acta Mater. Vol. 46 (1998), p. 6351.
[93] B. Baudelet, M.C. Dang, F. Bordeux: Scripta Metall. Mater. Vol. 26 (1992), p. 573.
[93] M. Mabuchi, K. Higashi, T. Imai, K. Kubo: Scripta Metall. Vol. 25 (1991), p. 1675.
[94] B. Straumal, O. Kogtenkova, S. Protasova, A. Mazilkin, P. Zieba, T. Czeppe, J. Wojewoda-Budka, M. Faryna: Mater. Sci. Eng. A 495 Vol. (2008), p. 126.
[95] V.K. Gupta, D.H. Yoon, H.M. Meyer, J. Luo: Acta. Mater. Vol. 55 (2007), p. 3131.
[96] J. Luo, V.K. Gupta, D.H. Yoon, H.M. Meyer: Appl. Phys. Lett. Vol. 87 (2005), p. 231902.
[97] V. Glebovsky, B. Straumal, V. Semenov, V. Sursaeva, W. Gust: Plansee Sem. Proc. Vol. 13 (1993), p. 429.
[98] V.G. Glebovsky, B.B. Straumal, V.N. Semenov, V.G. Sursaeva, W. Gust: High Temp. Mater. & Processes Vol. 13 (1994), p. 67.
[99] E. Rabkin, D. Weygand, B. Straumal, V. Semenov, W. Gust, Y. Bréchet: Phil. Mag. Lett. Vol. 73 (1996), p. 187.
[100] B. Straumal, V. Semenov, V. Glebovsky, W. Gust: Defect Diff. Forum Vols. 143–147 (1997), p. 1517.
[101] V.N. Semenov, B.B. Straumal, V.G. Glebovsky, W. Gust: J. Crystal Growth Vol. 151 (1995), p. 180.
[102] M. Matsuoka: Jap. J. Appl. Phys. Vol. 10 (1971), p. 736.
[103] L.M. Levinson, H.R. Philipp: Amer. Ceram. Soc. Bull. Vol. 65 (1986), p. 639.
[104] T.K. Gupta: J. Amer. Ceram. Soc. Vol. 73 (1990), p. 1817.
[105] F. Greuter, G. Blatter: Semicond. Sci. Technol. Vol. 5 (1990), p. 111.
[106] B. Bhushan, S.C. Kashyap, K.L. Chopra: J. Appl. Phys. Vol. 52 (1981), p. 2932.
[107] J. Wong: J. Appl. Phys. Vol. 51 (1980), p. 4453.
[108] H. Wang, Y.-M. Chiang: J. Amer. Ceram. Soc. Vol. 81 (1998), p. 89.
[109] J. Wong: J. Amer. Ceram. Soc. Vol. 57 (1974), p. 357.
[110] J. Wong, W.G. Morris: Amer. Ceram. Soc. Bull. Vol. 53 (1974), p. 816.
[111] F. Greuter: Solid State Ionics Vol. 75 (1995), p. 67.
[112] W.D. Kingery, J.B. van der Sande, T. Mitamura: J. Amer. Ceram. Soc. Vol. 62 (1979), p. 221.
[113] E. Olsson, L.K.L. Falk, G.L. Dunlop: J. Mater. Sci. Vol. 20 (1985), p. 4091.
[114] E. Olsson, G.L. Dunlop: J. Appl. Phys. Vol. 66 (1989), p. 3666.
[115] J.-R. Lee, Y.-M. Chiang, G. Ceder: Acta Mater. Vol. 45 (1997), p. 124.
[116] M. Safronov, V.N. Batog, T.V. Stepanyuk, P.M. Fedorov: Russ. J. Inorg. Chem. Vol. 16 (1971), p. 460.
[117] J.P. Guha, S. Kunej, D. Suvorov: J. Mater. Sci. Vol. 39 (2004), p. 911.
[118] D.R. Clarke: J. Appl. Phys. Vol. 49 (1978), p. 2407.

[119] W. Onreabroy, N. Sirikulrat, A.P. Brown, C. Hammond, S.J. Milne: Solid State Ionics Vol. 177 (2006), p. 411.
[120] J. Gambino, D. Kingery, G. Pike, L. Levinson, H.J. Philipp: J. Am. Ceram. Soc. Vol. 72 (1989), p. 642.
[121] J.R. Lee, Y.M. Chiang: Solid State Ionics Vol. 75 (1995), p. 79.
[122] H.L. Tuller, A.S. Nowick: J. Electrochem. Soc.Vol. 122 (1975), p. 255.
[123] M. Filal, C. Petot, M. Mokchah, C. Chateau, J.L. Charpentier: Solid State Ionics, Vol. 80 (1995), p. 27.
[124] G. Petot-Ervas, C. Petot: Solid State Ionics, Vol. 117 (1999), p. 27.
[125] A. Rizea, D. Chirlesan, C. Petot, G. Petot-Ervas: Solid State Ionics, Vol. 146 (2002), p. 341.
[126] S.P.S. Badwal: Solid State Ionics, Vol. 76 (1995), p. 67.
[127] M. Aoki, Y. Chiang, I. Kosacki, L.J. Lee, H. Tuller, Y. Liu: J. Amer. Ceram. Soc., Vol. 79 (1996), p. 1169.
[128] P. Mondal, A. Klein, W. Jaegermann, H. Hahn: Solid State Ionics, Vol. 118 (1999), p. 331.
[129] G. Xu, Y.W. Zhang, C.S. Liao, C.H. Yan: Solid State Ionics, Vol. 166 (2004), p. 391.
[130] E .P. Butler, J. Drennan: J. Amer. Ceram. Soc., Vol. 65 (1982), p. 474.
[131] M. Godickemier, B. Michel, A. Orlinkas, P. Bohac, K. Sasaki, L. Gauckler, H. Henrich, P. Schwander, G. Kostorz, H. Hofmann, O. Frei: J. Mater. Res. Vol. 9 (1994), p. 1228.
[132] A.J. Feighery, J.T.S. Irvine: Solid State Ionics Vol. 121 (1999), p. 209.
[133] A. Yuzaki, A. Kishimoto: Solid State Ionics Vol. 116 (1999), p. 47.
[134] X. Guo, C.Q. Tang, R.Z. Yuan: J. Eur. Ceram. Soc. Vol. 15 (1995), p. 25.
[135] T.S. Zhang, J. Ma, L.B. Kong, S.H. Chan, P. Hing, J.A. Kilner: Solid State Ionics Vol. 167 (2004), p. 203.
[136] A. Tschöpe, S. Kilassonia, R. Birringer: Solid State Ionics Vol. 173 (2004), p. 57.
[137] L. Gremillard, T. Epicier, J. Chevalier, G. Fantozzi: J. Eur. Cer. Soc. Vol. 25 (2005), p. 875.
[138] J.Y. Park, G.M.Choi: Solid State Ionics Vols. 154–155 (2002), p. 53.
[139] M.-B. Park, N.-H. Cho: Solid State Ionics Vols. 154–155 (2002), p. 407.
[140] I. MacLaren, R.M. Cannon, M.A. Gülgün, R. Voytovich, N. Popescu-Pogrion, C. Scheu, U. Töffner, M Rühle: J. Am. Ceram. Soc. Vol. 86 (2003), p. 650.
[141] S.J. Dillon, M.P. Harmer: J. Eur. Ceram. Soc. Vol. 28 (2008), p. 1485.
[142] M. Baram, S.H. Garofalini, W.D. Kaplan: Acta Mater. Vol. 59 (2011), p. 5710.
[143] M. Baram, D. Chatain, W.D. Kaplan: Science Vol. 332 (2011), p. 206.
[144] P. Švančárek, D. Galusek, F. Loughran, A. Brown, R. Brydson, A. Atkinson, F. Riley: Acta Mater. Vol. 54 (2006), p. 4853.
[145] M. Yoshiya, I. Tanaka, H. Adachi: J. Eur. Ceram. Soc. Vol. 32 (2012), p. 1301.
[146] T.M. Shaw: J. Am. Ceram. Soc. Vol. 62 (1979), p. 585.
[147] K.M. Knowles, S. Turan: Mater. Sci. Forum Vols. 207–209 (1996), p. 353.
[148] I. Tanaka, H.J. Kleebe, M.K. Cinibulk, J. Bruley, D.R. Clarke, M. Rühle: J. Am. Ceram. Soc. Vol. 77 (1994), p. 911.
[149] I. Tanaka, K. Igashira, H.J. Kleebe, M. Rühle: J. Am. Ceram. Soc. Vol. 77 (1994), p. 275.
[150] G.S. Painter, P.F. Becher, H.J. Kleebe, G. Pezzotti: Phys. Rev. B Vol. 65 (2002), p. 064113.
[151] H. Gu, R.M. Cannon, M. Rühle: J. Mater. Res. Vol. 13 (1998), p. 376.
[152] H. Gu, M. Čeh, S. Stemmer, H. Müllejans, M. Rühle: Ultramicroscopy Vol. 59 (1995), p. 215.
[153] M. Yoshiya, I. Tanaka, H. Adachi, R.M. Cannon: Int. J. Mater. Res. Vol. 101 (2010), p. 57.
[154] S. Ii, C. Iwamoto, K. Matsunaga, T. Yamamoto, M. Yoshiya, Y. Ikuhara: Philos. Mag. Vol. 84 (2004), p. 2767.
[155] A. Ziegler, J.C. Idrobo, M.K. Cinibulk, C. Kisielowski, N.D. Browning, R.O. Ritchie: Science Vol. 306 (2004), p. 1768.
[156] N. Shibata, S.J. Pennycook, T.R. Cosnell, G.S. Painter, W.A. Shelton, P.F. Becher: Nature Vol. 428 (2004), p. 730.

[157] G.B. Winkelman, C. Dwyer, T.S. Hudson, D. Nguyen-Manh, M. Döblinger, R.L. Satet, M.J. Hoffmann, D.J.H. Cockayne: Appl. Phys. Lett. Vol. 87 (2005), p. 061911.
[158] N. Shibata, G.S. Painter, P.F. Becher, S.J. Pennycook: Appl. Phys. Lett. Vol. 89 (2006), p. 051908.
[159] Y. Jiang, S.H. Garofalini: Acta Mater. Vol. 59 (2011), p. 5368.
[160] S. Bhattacharyya, C.T. Koch, M. Rühle: J. Ceram. Soc. Japan Vol. 114 (2006), p. 1005.
[161] H.J. Kleebe, M.K. Cinibulk, R.M. Cannon, M. Rühle: J. Am. Ceram. Soc. Vol. 76 (1993), p. 1969.

Recent Advances in Mass Transport in Engineering Materials
10.4028/www.scientific.net/DDF.333

Pseudopartial Grain Boundary Wetting: Key to the Thin Intergranular Layers
10.4028/www.scientific.net/DDF.333.175